AIAA JOURNAL
Vol. 32, No. 10, October 1994

Comparison of Two Methods for Solving Three-Dimensional Unsteady Compressible Viscous Flows

Ray Hixon,* Fu-Lin Tsung,* and L. N. Sankar†
Georgia Institute of Technology, Atlanta, Georgia 30332

Numerical solutions of three-dimensional unsteady compressible viscous flows for several cases have been obtained using two time-marching procedures: a noniterative alternating direction implicit (ADI) scheme and a generalized minimal residual (GMRES) method using an iterative version of the ADI scheme as a preconditioner. Results obtained are compared with each other and also with experimental data. It is found that the GMRES scheme can reduce CPU time by as much as 60% compared to the noniterative ADI scheme.

Introduction

DURING the past two decades, there has been significant progress in the field of numerical simulation of unsteady compressible viscous flows. At present, a wide variety of solution techniques exist such as transonic small disturbance analyses,[1–3] transonic full potential equation-based methods,[4–6] unsteady Euler solvers,[7,8] and unsteady Navier-Stokes solvers.[9–12] These advances have been made possible by developments in three areas: 1) improved numerical algorithms, 2) automation of body-fitted grid generation schemes, and 3) advanced computer architectures with vector and parallel processing features.

Despite these advances, numerical simulation of unsteady viscous flows still remains a computationally intensive problem, especially in three dimensions. For example, an unsteady Navier-Stokes simulation of a helicopter blade in forward flight may require over 30,000 time steps for a full revolution of the rotor.[10] In other unsteady flows, such as the high angle-of-attack flow past fighter aircraft configurations, a systematic parametric study of the flow is presently not practical due to the very large CPU time needed for the simulations.[13] Thus, it is clear that significant improvements to the existing algorithms or dramatic improvements in computer architectures will be needed before unsteady three-dimensional viscous flow analyses become practical day-to-day engineering tools.

One numerical scheme that has been of recent interest is the generalized minimal residual (GMRES) method originally proposed by Saad and Schultz.[14] This procedure uses a conjugate gradientlike method to improve the performance of existing flow solvers. GMRES was added to a variety of steady flow solvers by Wigton et al.[15] and to an unstructured grid solver by Venkatakrishnan and Mavriplis.[16] Saad has also used a Krylov subspace method on a steady, incompressible Navier-Stokes problem and an unsteady one-dimensional wave propagation equation.[17] GMRES has also been used to accelerate two-dimensional unsteady viscous flow computations.[18]

In this work, the GMRES scheme is being considered as a candidate for reducing the CPU time requirements for unsteady three-dimensional compressible viscous flow calculations; from previous experience with two-dimensional calculations, significant reductions in the CPU time are possible. The GMRES method is tested on structured grids, although the method is flexible enough for extension to unstructured grids. The results given are only for implementation on a Cray Y-MP, but the two-dimensional solver has been implemented on an Intel iPSC/860 MIMD parallel machine as well.

Presented as Paper 93-0537 at the AIAA 31st Aerospace Sciences Meeting, Reno, NV, Jan. 11–14, 1993; received July 1, 1993; revision received Nov. 16, 1993; accepted for publication Nov. 26, 1993.

*Graduate Research Assistant, School of Aerospace Engineering. Member AIAA.

†Professor, School of Aerospace Engineering. Senior Member AIAA.

Mathematical and Numerical Formulation

Iterative Alternating Direction Implicit Formulation

The unsteady, three-dimensional, compressible alternating direction implicit (ADI) code used in this study solves the Navier-Stokes equations with an implicit/explicit hybrid scheme.[19] The user is given the choice of using second- or fourth-order-accurate central differences for the spatial derivatives, and a first-order backward difference is used for the time derivative. For these investigations, second-order-accurate differences are used for the spatial derivatives.

The iterative ADI scheme advances the flowfield by numerically integrating the Navier-Stokes equations at each time step

$$q_t + E_x + F_y + G_z = R_x + S_y + T_z \tag{1}$$

where q is the vector of conserved flow properties. In Eq. (1), E, F, and G are the convective terms, and R, S, and T are the viscous terms.

At each time step, the following equation is iteratively solved:

$$[I + \Delta t \partial_x A^{n+1,k} + \varepsilon_x]\,[I + \Delta t \partial_z C^{n+1,k} + \varepsilon_z]\,\{\Delta q\}$$
$$= -\Delta t\left(\frac{q^{n+1,k} - q^n}{\Delta t}\right) + \Delta t\,[\partial_x(R-E) + \partial_x(S-F) + \partial_x(T-G)]^{n+1,k} \tag{2}$$

where

$$\Delta q = q^{n+1,k+1} - q^{n+1,k} \tag{3}$$

In these equations, n refers to the time level and k to the iteration level. To evaluate Eq. (2), it is necessary to have both the flowfield at the old time level q^n and an approximation $q^{n+1,k}$ for the flowfield at the new time level. For these calculations, the initial guess for the flowfield at the new time level $q^{n+1,0}$ is set equal to the values at the last time level q^n.

In Eq. (2), ε_x and ε_z are implicit artificial dissipation operators defined as

$$\varepsilon_x = \kappa \Delta t\, \Delta x^2\, \partial_{xx}$$
$$\varepsilon_z = \kappa \Delta t\, \Delta z^2\, \partial_{zz} \tag{4}$$

where κ is a user-supplied parameter. Since the left-side operators are invertible, Eq. (2) may formally be written as

$$q^{n+1,k+1} = q^{n+1,k} + \Delta q = q^{n+1,k} + M(q^{n+1,k}) \tag{5}$$

A noniterative ADI scheme simply has only one iteration performed at each time step.

Generalized Minimal Residual Formulation

Equation (3) may be rewritten as

$$\boldsymbol{q}^{n+1,k+1} = \boldsymbol{q}^{n+1,k} + \Delta\boldsymbol{q} = \boldsymbol{q}^{n+1,k} + a\boldsymbol{d} \tag{6}$$

where $\boldsymbol{d}$ is a unit vector

$$\boldsymbol{d} = \frac{\Delta\boldsymbol{q}}{\|\Delta\boldsymbol{q}\|} \tag{7}$$

and a is the magnitude of the correction vector

$$a = \|\Delta\boldsymbol{q}\| \tag{8}$$

In other words, using the latest guess for the solution at the new time level, the original code computes a corrected solution $q^{n+1,k+1}$, which is equivalent to moving a distance a in direction d from the initial point $q^{n+1,k}$.

In a two-dimensional problem, the Δq vector has a length equal to the total number of flow variables in the computation [i.e., ($i$max $\times$ $k$max $\times$ 4) for two dimensions]. The correction vector may change only one flow variable at one point in the flowfield (e.g., ρu at $i = 5$, $k = 13$), and leave the rest alone. This is one possible direction that the code could move in. If another variable at another point is changed instead (e.g., ρ at $i = 120$, $k = 2$), this would result in the code moving in a second direction which is orthogonal to the first. Thus, it can be seen that there are a total of ($i$max $\times$ $k$max $\times$ 4) possible orthogonal directions in a two-dimensional problem, and ($i$max $\times$ $j$max $\times$ kmax $\times$ 5) directions in three dimensions.

The iterative ADI code considers only one direction at a time. In other words, it starts from an initial point, computes a single likely direction, and moves some distance in this direction to the next point, where the same process is repeated.

The GMRES solver works in a different way. GMRES computes the slope of the residual in a number of orthogonal directions from the initial point and uses this information to make a more informed move from the initial point. In this procedure, the underlying iterative solver serves as a "black box" function evaluator (i.e., given a set of input flow properties, the solver sends back an updated set of flow properties) to provide GMRES with information to compute the set of flow properties that will satisfy Eq. (2).

Note that the GMRES implementation does not change with the number of equations or the method of solution of the underlying code. The only change in GMRES for two dimensions to three dimensions is the length of the vectors; there is no change in the GMRES code between, for example, ADI and lower-upper symmetric Gauss-Seidel solvers.

Following closely the development of Wigton et al. in Ref. 15, each GMRES(J) (J refers to the number of search directions used) step follows the ensuing procedure.

First, the initial direction is computed as

$$\boldsymbol{d}_1 = M(\boldsymbol{q}^{n+1,0}) \tag{9}$$

and normalized as

$$\boldsymbol{d} = \frac{\boldsymbol{d}_1}{\|\boldsymbol{d}_1\|} \tag{10}$$

Thus, the first direction is the direction in which the underlying solver would have moved from the initial point.

To compute the remaining search directions ($j = 1, 2, \ldots, J-1$), the GMRES solver first moves a small distance in the jth direction and calls the underlying solver to compute the residual at this point. Then, the slope of the residual in the jth direction can be numerically evaluated using

$$\bar{M}(\boldsymbol{q};\boldsymbol{d}) = \frac{M(\boldsymbol{q}+\varepsilon\boldsymbol{d}) - M(\boldsymbol{q})}{\varepsilon} \tag{11}$$

where ε is taken to be some small number. Numerical studies were performed to determine an optimum value for ε, and the GMRES procedure was very insensitive to this parameter. In this work, ε is taken to be 0.001.

Taking the dot product of this derivative with a unit direction vector yields the component of the derivative in that direction,

$$b_{ij} = [\bar{M}(\boldsymbol{q}^{n+1,0};\boldsymbol{d}_j), \boldsymbol{d}_i] \tag{12}$$

If the components of the derivative in all of the known directions are subtracted from the derivative, what results is a new direction vector that is orthogonal to all of the known directions

$$\boldsymbol{d}_{j+1} = \bar{M}(\boldsymbol{q}^{n+1,0};\boldsymbol{d}_j) - \sum_{i=1}^{j} b_{ij}\boldsymbol{d}_i \tag{13}$$

Normalizing the new direction vector will give the component of the derivative in the new direction

$$b_{j+1,j} = \|\boldsymbol{d}_{j+1}\| \tag{14}$$

and the unit vector in the new direction may finally be computed as

$$\boldsymbol{d}_{j+1} = \frac{\boldsymbol{d}_{j+1}}{b_{j+1,j}} \tag{15}$$

Since GMRES uses the underlying flow solver to determine the search directions, the success and speed of the GMRES solution method depends greatly on the original flow solver's ability to help define useful direction vectors and, hence, a subspace that contains many of the error components.

After obtaining the search directions, the solution vector is updated using

$$\boldsymbol{q}^{n+1,k+1} = \boldsymbol{q}^{n+1,k} + \sum_{j=1}^{J} a_j\boldsymbol{d}_j \tag{16}$$

where the undetermined coefficients a_j are chosen to minimize

$$\|M(\boldsymbol{q}^{n+1,k+1})\|^2 = \left\|M\left(\boldsymbol{q}^{n+1,k} + \sum_{j=1}^{J} a_j\boldsymbol{d}_j\right)\right\|^2$$

$$\cong \left\|M(\boldsymbol{q}^{n+1,k}) + \sum_{j=1}^{J} a_j\bar{M}(\boldsymbol{q}^{n+1,k};\boldsymbol{d}_j)\right\|^2 \tag{17}$$

Results

Both the ADI and GMRES solvers have been applied to the three cases discussed subsequently. A $121 \times 19 \times 41$ grid was used for all viscous calculations, whereas a $121 \times 19 \times 21$ grid was used for the inviscid case. All timings and memory requirements given are from the NASA Langley Cray Y-MP using a single processor. All of the residuals shown are computed using the L_2 norm. All of the experimental results cited are from Tijdeman et al.[20]

The GMRES solver was first validated by calculating a steady viscous transonic flow about an F-5 wing. It was found that the GMRES solver required additional implicit artificial dissipation compared to the ADI code, but the solution was identical to that of the ADI code and the convergence rate was comparable. Since computing unsteady flow cases was the prime objective of this work, no further research was performed in this area.

Unsteady Viscous Flow About an F-5 Wing with an Oscillating Flap

The second case investigated is the unsteady flow over an F-5 wing with a harmonically oscillating trailing-edge control surface, hinged at $x/c = 0.82$. The trailing edge oscillates at a frequency of

20 Hz, with $M_\infty = 0.90$, $Re = 11 \times 10^6$, $\alpha_{wing} = 0.0$ deg, and $\alpha_{flap} = \pm 0.5$ deg. Here, α_{wing} represents the angle of attack of the wing, and α_{flap} represents the maximum angle of attack of the trailing-edge flap. The flap deflection was modeled by appropriate shearing of the grid aft of the flap hinge, using grid motion terms to account for the movement of the grid points.

For brevity, computed results at only one experimental span station are shown ($y = 0.181$). Since the oscillation of the trailing-edge flap is harmonic, the pressure coefficient is assumed also to vary harmonically and is decomposed into an in-phase component (the real component) and an out-of-phase component (the imaginary component). In the comparison, the real and imaginary components of the pressure coefficient are defined as

$$(C_p)_{\text{imaginary}} = \frac{(C_p)_{\omega t = \pi} - (C_p)_{\omega t = 0}}{2\Delta\alpha_{\text{flap}}}$$

$$(C_p)_{\text{real}} = \frac{(C_p)_{\omega t = 3\pi/2} - (C_p)_{\omega t = \pi/2}}{2\Delta\alpha_{\text{flap}}} \tag{18}$$

Table 1 Unsteady transonic viscous flow computer time requirements

	Memory, mW	CPU time, s	CPU, % of ADI
ADI	3.66	5533	100
GMRES (5/10)	7.72	3952	71
GMRES (5/20)	7.72	2002	36

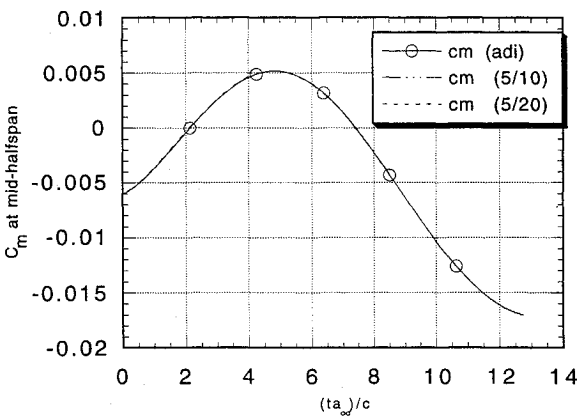

Fig. 1 Comparison of three-dimensional GMRES with ADI results for the mid-half-span moment coefficient on an F-5 wing with an oscillating trailing-edge flap: $M_\infty = 0.9$, $f = 20$ Hz, $\alpha = 0.0$ deg, $\alpha_{flap} = 0.5$ deg, and $Re = 11 \times 10^6$.

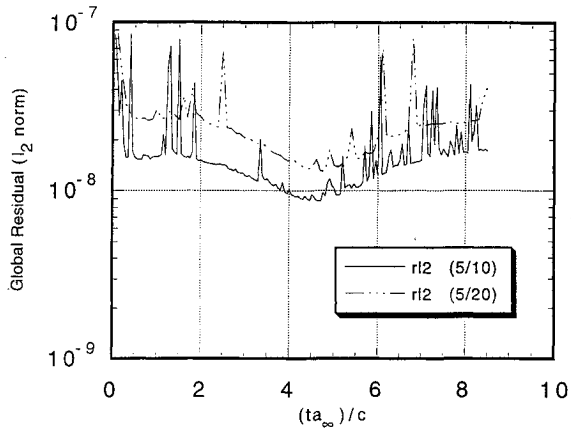

Fig. 2 Effect of time step on the GMRES (5/x) results for the global residual of the transonic viscous flow about an F-5 wing with an oscillating trailing-edge flap: $M_\infty = 0.9$, $f = 20$ Hz, $\alpha = 0.0$ deg, $\alpha_{flap} = 0.5$ deg, and $Re = 11 \times 10^6$.

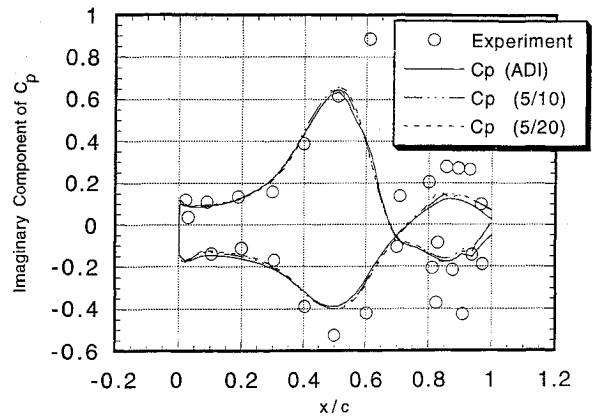

Fig. 3 Comparison of three-dimensional GMRES results for the imaginary component of the pressure coefficient on an F-5 wing with an oscillating trailing-edge flap: $M_\infty = 0.9$, $f = 20$ Hz, $\alpha = 0.0$ deg, $\alpha_{flap} = 0.5$ deg, $Re = 11 \times 10^6$, $y = 0.181$.

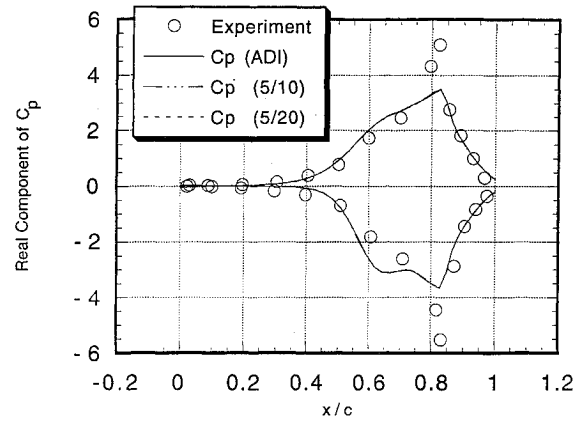

Fig. 4 Comparison of three-dimensional GMRES results for the real component of the pressure coefficient on an F-5 wing with an oscillating trailing-edge flap: $M_\infty = 0.9$, $f = 20$ Hz, $\alpha = 0.0$ deg, $\alpha_{flap} = 0.5$ deg, $Re = 11 \times 10^6$, $y = 0.181$.

The data presented using Eq. (18) are for the initial 3/4 cycle of oscillation. Because of the existence of transients in the flowfield, it is somewhat unfair to compare these results with experimental results that do not include these transients. Previous studies with the noniterative ADI solver indicate that much better correlation with the experimental data can be achieved if the solution is allowed to march more than one cycle or until no discrepancies are found between successive cycles of oscillation. Since the object of this investigation was to compare the GMRES code with the original ADI code, and not directly with experiment, only the initial 3/4 cycle was run.

The preconditioner for the GMRES calculation was the iterative ADI solver described earlier. Within each time level, local time steps are used for the iteration. That is, Eq. (2) is replaced by

$$[I + \Delta t_{i,j,k}\partial_x A^{n+1,k} + \varepsilon_x]\,[I + \Delta t_{i,j,k}\partial_z C^{n+1,k} + \varepsilon_z]\,\{\Delta q\}$$

$$= -\Delta t_{i,j,k}\left(\frac{q^{n+1,k} - q^n}{\Delta t}\right) + \Delta t_{i,j,k}\,[\partial_x (R - E)$$

$$+ \partial_x (S - F) + \partial_x (T - G)]^{n+1,k} \tag{19}$$

where $\Delta t_{i,j,k}$ is the local time step, which is a function of the grid and local flow conditions. Note that only one iteration is performed for each function evaluation.

For initial comparisons, a five direction GMRES run was made at five times the ADI time step [GMRES (5/5), where the first number designates the number of directions, and the second num-

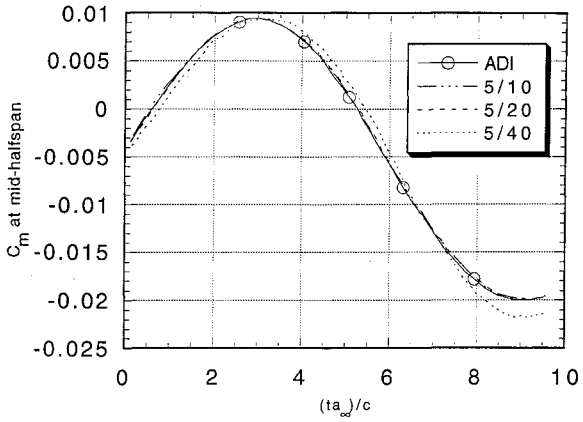

Fig. 5 Comparison of three-dimensional GMRES (5/x) with ADI results for the mid-half-span moment coefficient of an F-5 wing undergoing modal vibration: M_∞= 0.9, f = 20 Hz, α = 0.0 deg, α_{max} = 0.5 deg.

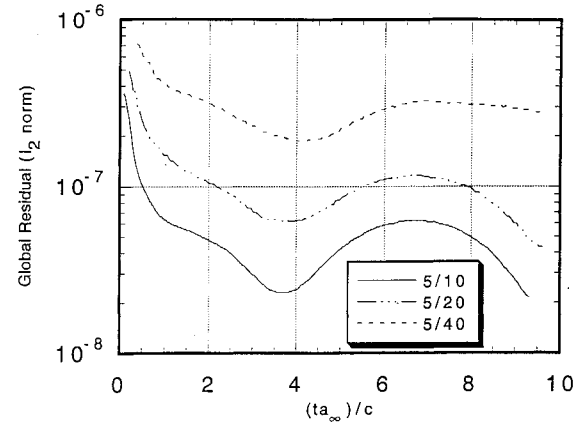

Fig. 6 Comparison of three-dimensional GMRES (5/x) global residual histories for the inviscid flow about an F-5 wing undergoing modal vibration: M_∞= 0.9, f = 20 Hz, α = 0.0 deg, α_{max} = 0.5 deg.

ber is the time step factor], and the GMRES solution followed the ADI solution exactly.

After the initial validation, the GMRES time step factor was increased to numerically determine the largest time step that can be used without large loss of accuracy due to temporal discretization errors. To carry out this task, GMRES (5/10) and (5/20) runs were performed. Both the (5/10) and (5/20) runs gave good results and provided significant speedups, but the (5/20) results showed some degradation in solution accuracy.

The CPU time and memory required for the ADI and three GMRES runs are shown in Table 1. It should be noted that the CPU time of the GMRES (5/20) run is only 36% of that required by the underlying ADI code, although the solution is very nearly as good. This means that a designer can use the GMRES code for three different cases for the same amount of CPU time required to run the ADI code for one case. This is a significant savings.

Time histories of the mid-half-span moment coefficient for two GMRES runs are compared in Fig. 1. It is seen that the results are identical to that of the ADI solver. Figure 2 shows the residual histories of the GMRES runs. These residuals are the global residual at the end of each GMRES step, which illustrates the total error at the end of each time step. Figures 3 and 4 compare the imaginary and real components of the pressure coefficients with both experiment and the ADI solver at the y = 0.181 span station. It is seen that even with only 3/4 of a cycle of oscillation computed, the shock locations agree very well with experiment and the pressure coefficient is qualitatively correct.

It should be noted that the imaginary component of the pressure coefficient is measured at the times when the flap is moving the fastest. Therefore, the imaginary (out-of-phase) component of the pressure coefficient is a better measure of the time accuracy of the code. Conversely, the real (in-phase) component of the pressure coefficient is measured when the flap is moving the slowest and is a much looser measure of time accuracy.

This is illustrated in Figs. 3 and 4. In Fig. 3, which shows the imaginary (out-of-phase) component of the pressure coefficient, the GMRES (5/20) answer differs slightly from that of the ADI code, mainly near the rear of the airfoil section. In Fig. 4, which shows the real (in-phase) component of the pressure coefficient, the GMRES (5/20) answer is indistinguishable from that of the ADI code. For this reason, the imaginary component of the pressure coefficient was weighed more heavily in determining the time accuracy of the GMRES code.

Unsteady Flow About an F-5 Wing in Modal Vibration

The third case investigated is the unsteady inviscid flow about an F-5 wing undergoing modal vibration. Since this wing is both tapered and swept, it cannot have either a pure pitching or pure bending mode of vibration; instead, it will have a mode of vibration which combines both bending and torsion. In Tijdeman's experiments,[20] accelerometers were mounted on the wing and used to measure the local accelerations of the wing surface. The accelerometer data were then integrated twice to determine an analytic function for the mode shape of the wing; this function was used as an input to the flow solver.

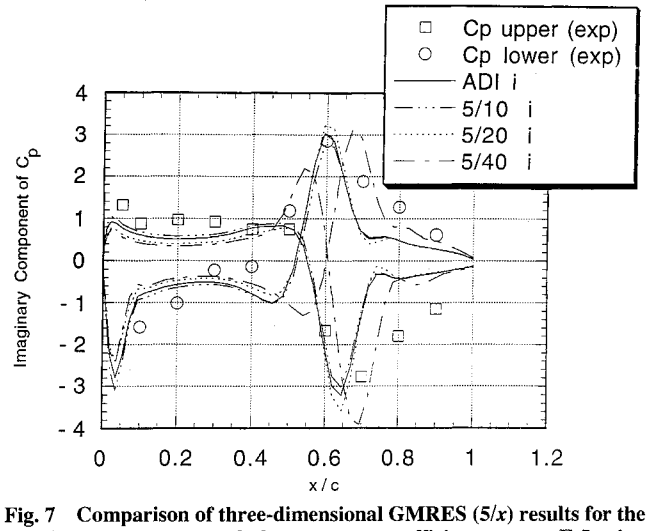

Fig. 7 Comparison of three-dimensional GMRES (5/x) results for the imaginary component of the pressure coefficient on an F-5 wing undergoing modal vibration: M_∞= 0.9, f = 20 Hz, α = 0.0 deg, α_{max} = 0.5 deg, y = 0.181.

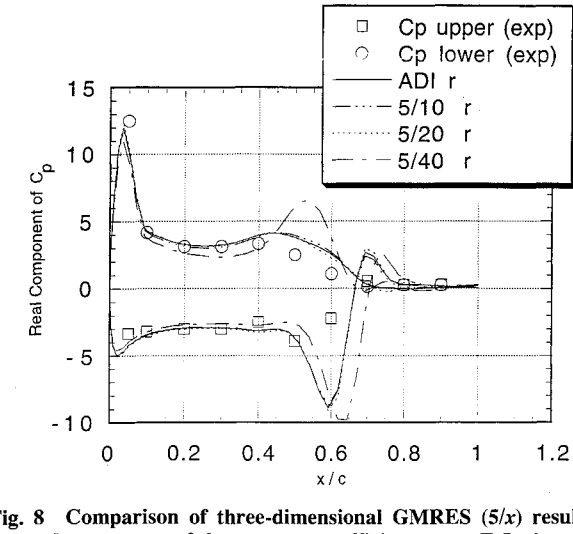

Fig. 8 Comparison of three-dimensional GMRES (5/x) results for the real component of the pressure coefficient on an F-5 wing undergoing modal vibration: M_∞= 0.9, f = 20 Hz, α = 0.0 deg, α_{max} = 0.5 deg, y = 0.181.

In this case, $M_\infty = 0.90$, $\alpha_{wing} = 0.0$ deg, and $\alpha_{oscillation} = \pm 0.5$ deg, with an oscillation frequency of 40 Hz (reduced frequency of 0.275). From the experimental data, the amplitude of the wing surface deformation was found to be:

$$w(x, y) = -0.329 + 0.977x - 0.088y + 0.244xy - 0.077y^2 - 0.091xy^2 \quad (20)$$

Equation (20) gives a pure angular displacement with the nondimensionalization performed such that the tangent of the angle of oscillation at experimental span station 2 is equal to one. The pressure coefficient may be separated into real and imaginary components by using Eq. (18).

Again, the computational grid is sheared to model the motion of the wing. Given a maximum angular displacement specified at station 2, Eq. (20) may be scaled to give the relative displacements at the other spanwise computational stations. Since the wing is assumed to be undergoing a simple harmonic vibration, the displacement of the wing is thus specified at all time levels.

Initially, the original ADI code was run for 3/4 of a cycle of oscillation to establish a baseline solution to compare to the GMRES solutions. The ADI code required 1.5 mW of memory to run and took 698 CPU s to complete 3/4 of a cycle of oscillation. Again, it should be noted that the original ADI code compares much better with experimental data if the solution is allowed to run over several cycles of oscillation to let the transients decay. Since this simulation requires very little CPU time, it was used to more thoroughly determine the effects of both the time step and the error at each step on the solution accuracy.

Again, GMRES (5/5) was used as an initial run, and the results were identical to the original ADI code. To limit the GMRES memory requirements, only five directions were employed. The five-direction GMRES code required 4.1 mW of memory to run (2.73 times larger than the original ADI code).

Effects of Time Step on Solution with Five Directions

At this point, the time step was increased to determine the maximum time steps possible with five GMRES directions. Time steps that were 10, 20, and 40 times larger than those used by the ADI scheme were tried.

Table 2 Unsteady inviscid transonic flow computer requirements

	Memory, mW	CPU time, s	CPU, % of ADI
ADI	1.4	698	100
GMRES (5/10)	4.1	513	74
GMRES (5/20)	4.1	265	38
GMRES (5/40)	4.1	131	19

Table 3 CPU time and memory usage for ADI and GMRES calculations for flow about an F-5 wing in modal vibration

	Memory, mW	CPU time, s	CPU, % of ADI
ADI	1.4	698	100
GMRES (5/40)-1	4.1	131	19
GMRES (5/40)-2	4.1	262	38
GMRES (5/40)-3	4.1	390	56
GMRES (5/40)-4	4.1	525	75

Table 4 CPU time and memory usage for ADI and GMRES calculations for flow about an F-5 wing in modal vibration with fixed error magnitudes

	Memory, mW	CPU time, s	CPU, % of ADI
ADI	1.4	698	100
GMRES (5/10)-2	4.1	536	77
GMRES (5/20)-4	4.1	525	75

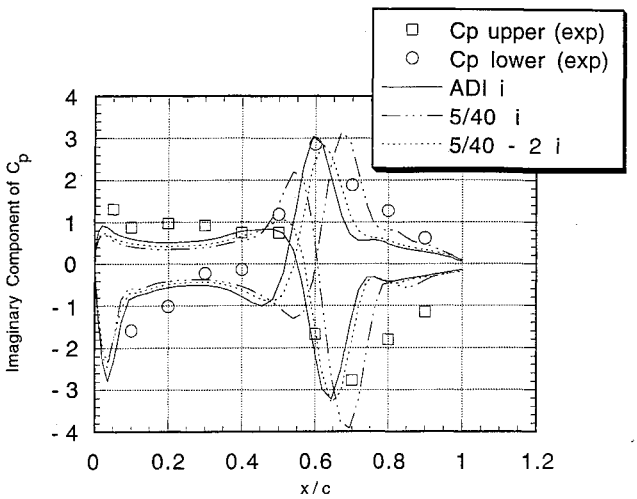

Fig. 9 Comparison of three-dimensional GMRES (5/40-x) results for the imaginary component of the pressure coefficient on an F-5 wing undergoing modal vibration: $M_\infty = 0.9$, $f = 20$ Hz, $\alpha = 0.0$ deg, $\alpha_{max} = 0.5$ deg, $y = 0.181$.

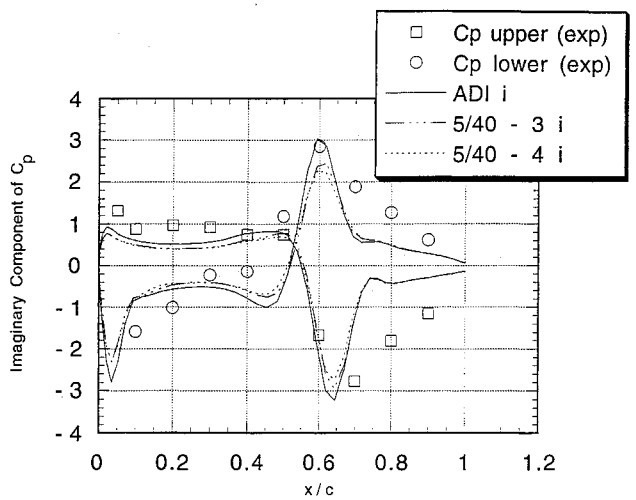

Fig. 10 Comparison of three-dimensional GMRES (5/40-x) results for the imaginary component of the pressure coefficient on an F-5 wing undergoing modal vibration: $M_\infty = 0.9$, $f = 20$ Hz, $\alpha = 0.0$ deg, $\alpha_{max} = 0.5$ deg, $y = 0.181$.

Since shock speed is sensitive to time step size and critically affects pitching moment, the mid-half-span moment coefficient histories were used to illustrate the effects of time step size on solution accuracy. Figure 5 shows that the moment coefficient, which is heavily influenced by shock location, is very different at 40 times the time step. To put this into perspective, the nondimensionalized ADI time step is

$$\Delta\tau = \frac{(a\Delta t)}{c} = 0.1 \quad (21)$$

One complete cycle (360 deg) of harmonic oscillation requires 1270 time steps, which is 0.283 deg of harmonic oscillation per time step. In this manner, it is seen that a GMRES (5/40) computation takes only 32 time steps per cycle, which is 11.33 deg of harmonic oscillation per step. With such a large time step, an error in shock speed is not entirely unexpected.

The residual histories of the GMRES (5/x) runs are shown in Fig. 6. Again, these residuals are the global residuals at the end of each GMRES step, which illustrates the total error at each time level. The real (in-phase) and imaginary (out-of-phase) components of the pressure coefficient at the $y = 0.181$ experimental

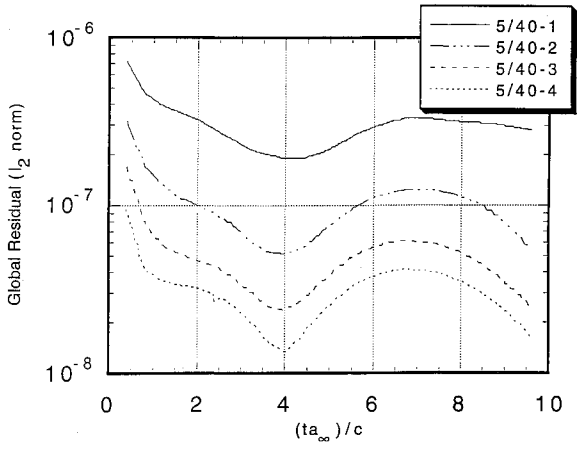

Fig. 11 Comparison of three-dimensional GMRES (5/40-x) global residual histories for the inviscid flow about an F-5 wing undergoing modal vibration: M_∞= 0.9, f = 20 Hz, α = 0.0 deg, α_{max} = 0.5 deg.

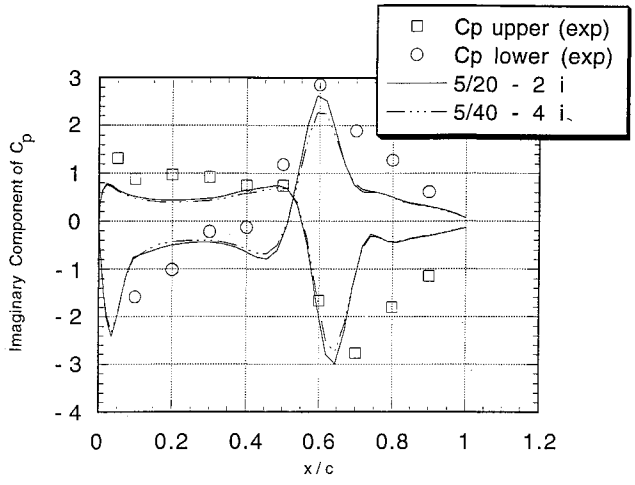

Fig. 12 Effect of time step on the GMRES result for the imaginary component of the pressure coefficient on an F-5 wing undergoing modal vibration: M_∞= 0.9, f = 20 Hz, α = 0.0 deg, α_{max} = 0.5 deg, y = 0.181.

spanwise station are shown in Figs. 7 and 8. These figures show that the solution begins to degrade slightly at 20 times the ADI time step, with the main differences being the pressure coefficient magnitudes at the shock. When the time step is multiplied by 40, both the shock location and magnitude are different.

The CPU time and memory required for the ADI and three GMRES runs are shown in Table 2.

Effect of Residual Magnitude on Solution Accuracy (Time Step Fixed)

The next area of investigation was to determine if a larger time step may be employed if the error is reduced more at each time step. Using the GMRES solver, there are two ways to accomplish this: either use more directions in each iteration or perform more than one GMRES iteration at each time step, using the result of the first GMRES iteration as the initial point for the next ("restart" GMRES).

Restart GMRES was chosen to keep the memory requirements constant. The restart code was employed on the GMRES (5/40) run, and up to four five-direction GMRES iterations were used per time step [referred to as GMRES (5/40)-1, (5/40)-2, etc.]. As more iterations were used and the error residual decreased the answer approached the ADI solution, but the magnitudes of the pressure peaks were reduced. However, the shock locations were predicted very well for both the real and imaginary components of the pressure coefficient. Figures 9 and 10 compare the imaginary components of the pressure coefficients computed by the restart GMRES (5/40)-x code. Figure 11 shows the residual histories of the GMRES (5/40)-x runs. The CPU time and memory required for the ADI and three GMRES runs are shown in Table 3.

Effect of Time Step on Solution Accuracy (Magnitude Fixed)

The next part of this investigation was to compare various GMRES runs which use different time steps but result in the same error magnitude. This would isolate the effect of the time step on the unsteady solution. To illustrate the results, a GMRES (5/20)-2 run is compared to a GMRES (5/40)-4 code that achieved an almost identical level of error residual. Figure 12 shows the imaginary component of the pressure coefficient. It is shown that even at this very large time step, the GMRES code still resolves the shock location well, but the amplitude of the shock is somewhat reduced as the time step is increased. It was hypothesized that this is due to error introduced by the first-order accuracy of the time derivative discretization. The CPU time and memory required for the ADI and GMRES runs are shown in Table 4.

Concluding Remarks

An existing three-dimensional Navier-Stokes/Euler solver has been successfully coupled to the GMRES algorithm, and the coupled solver has been used to study unsteady transonic flow past a fighter wing configuration. It is concluded that 1) for the cases tested, the GMRES/ADI solver can use time steps up to 20 times larger than that of the noniterative ADI solver, with a factor of 3 reduction in CPU time, and 2) to achieve the same degree of accuracy, it is more beneficial to use a restart GMRES scheme rather than increasing the number of directions (and the memory required) used for each GMRES iteration.

Acknowledgments

The GMRES research reported here was supported by a grant from NASA Langley Research Center, Grant NAG-1-1217. Woodrow Whitlow was the technical monitor. The F-5 oscillating flap simulations using the noniterative ADI code were done under the support of the Naval Air Warfare Center, Aircraft Division. Marvin Walters was the technical monitor.

References

[1]Borland, C. J., and Rizzetta, D., "Nonlinear Transonic Flutter Analysis," AIAA Paper 81-0608, Jan. 1981.

[2]Rizzetta, D. P., and Borland, C., "Numerical Solution of Unsteady Transonic Flow over Wings with Viscous-Inviscid Interaction," AIAA Paper 82-0352, Jan. 1982.

[3]Batina, J. T., "Unsteady Transonic Algorithm Improvements for Realistic Aircraft Applications," *Journal of Aircraft*, Vol. 26, No. 2, 1989, pp. 131–139.

[4]Sankar, L. N., Malone, J. B., and Tassa, Y., "An Implicit Conservative Algorithm for Steady and Unsteady Three Dimensional Transonic Potential Flows," AIAA Paper 81-1016, June 1981.

[5]Malone, J. B., and Sankar, L. N., "Application of a Three-Dimensional Steady and Unsteady Full Potential Method for Transonic Flow Computations," Flight Dynamics Lab., AFWAL-TR-84-3011, Dayton, OH, May 1984.

[6]Shankar, V., Ide, H., Gorski, J., and Osher, S., "A Fast, Time-Accurate Unsteady Full Potential Scheme," AIAA Paper 85-1512, July 1985.

[7]Pulliam, T. H., and Steger, J. L., "Implicit Finite-Difference Simulations of Three-Dimensional Compressible Flow," *AIAA Journal*, Vol. 18, No. 2, 1980, pp. 159–167.

[8]Batina, J. T., "Unsteady Euler Solutions Using Unstructured Dynamic Meshes," AIAA Paper 89-0115, Jan. 1989.

[9]Sankar, L. N., and Tang, W., "Numerical Solution of Unsteady Viscous Flow Past Rotor Sections," AIAA Paper 85-0129, Jan. 1985.

[10]Wake, B. E., and Sankar, L. N., "Solutions of the Navier-Stokes Equations for the Flow About a Rotor Blade," *Journal of the American Helicopter Society*, Vol. 34, April 1989, pp. 13–23.

[11]Rai, M. M., "Navier-Stokes Simulations of Rotor-Stator Interaction Using Patched and Overlaid Grids," AIAA Paper 85-1519, July 1985.

[12]Gatlin, B., and Whitfield, D. L., "An Implicit Upwind Finite Volume Scheme for Solving the Three-Dimensional Thin-Layer Navier-Stokes Equations," AIAA Paper 87-1149, June 1987.

[13]Kwon, O. J., and Sankar, L. N., "Viscous Flow Simulation of a Fighter

Aircraft," *Journal of Aircraft*, Vol. 29, No. 5, 1992, pp. 886–891.

[14]Saad, Y., and Schultz, M.H, "GMRES: A Generalized Minimum Residual Algorithm for Solving Nonsymmetric Linear Systems," *SIAM Journal Sci. Stat. Comp.*, Vol. 7, 1986, pp. 856–869.

[15]Wigton, L. B., Yu, N. J., and Young, D. P., "GMRES Acceleration of Computational Fluid Dynamics Codes," AIAA Paper 85-1494, June 1985.

[16]Venkatakrishnan, V., and Mavriplis, D. J., "Implicit Solvers for Unstructured Meshes," Inst. for Computer Applications in Science and Engineering, ICASE Rept. 91-40, Hampton, VA, May 1991.

[17]Saad, Y., and Semeraro, B. D., "Application of Krylov Exponential Propagation to Fluid Dynamics Equations," AIAA Paper 91-1567, June 1991.

[18]Hixon, R., and Sankar, L. N., "Application of a Generalized Minimal Residual Method to 2-D Unsteady Flows," AIAA Paper 92-0422, Jan. 1992.

[19]Tsung, F.-L., and Sankar, L. N., "Numerical Simulation of Flow Separation for Rotors and Fixed Wings," AIAA Paper 92-0635, 1992.

[20]Tijdeman, H., et al., "Results of Transonic Wind Tunnel Measurements on an Oscillating Wing with External Stores," National Aerospace Lab., NLR TR 78030U, The Netherlands, 1978.